

Scaling of the proton density reduction scheme for the laser acceleration of proton beams with a narrow energy spread

A P L Robinson¹, P Gibbon², S M Pfotenhauer³, O Jäckel³ and J Polz³

¹ Central Laser Facility, STFC Rutherford-Appleton Laboratory, Chilton, Didcot, Oxfordshire, OX11 0QX, UK

² Juelich Supercomputing Centre, Institute for Advanced Simulation, Forschungszentrum Jülich GmbH, D-52425, Jülich, Germany

³ Institute of Optics and Quantum Electronics, Friedrich Schiller University, Max-Wien-Platz 1, 07743 Jena, Germany

Received 15 April 2008, in final form 2 June 2008

Published 7 January 2009

Online at stacks.iop.org/PPCF/51/024001

Abstract

The laser acceleration of proton beams with quasi-monoenergetic features in the energy spectra from microdot targets is investigated by numerical simulation. The formation of these spectral peaks is strongly dependent on the interplay between different ion species in the target. The scaling of the spectral peak's energy, and number of protons in the spectral peak, with both microdot composition and laser intensity is considered. Particular attention is given to determining the proton concentration below which the number of protons in the spectral peak rapidly diminishes. It is shown that at proton concentrations of $1-5n_{\text{crit}}$ a spectral peak is produced that reaches an energy up to 70% of the maximum proton energy, whilst still containing more protons than would be produced by a conventional target in this energy range.

1. Introduction

Recently a number of independent experiments have shown that there are a range of different methods for producing multi-MeV proton or ion beams with a narrow energy spread from ultraintense ($>10^{18} \text{ W cm}^{-2}$) laser–solid interactions. The experiments have each taken a different approach, e.g. microdot targets [1, 2], ultrathin carbon layers [3], deuterated water droplets [4] and laser driven micro-lens [5]. These experiments provided the first demonstrations of laser accelerated quasi-monoenergetic proton and ion beams. This has been viewed as an important step towards the technological application of laser accelerated ion beams. One such application is the use of laser accelerated ion beams for the treatment of tumours, although it has been pointed out that considerable further development of laser-based accelerators is required before this is possible [6]. Looking beyond these first experiments,

a number of theoretical studies indicate that it might be possible to produce monoenergetic proton beams by interactions in which the radiation pressure of the laser pulse dominates the acceleration process [7–9].

This paper is mainly concerned with the method employed by Schwoerer *et al* [1], i.e. microdot targets. In previous work the authors have suggested that the heavy ion species play an important role in the production of quasi-monoenergetic ions from microdot targets [10]. This built on even earlier work by the authors [11] and other researchers [12–15] on the creation of a narrow-energy-band population of protons close to the electrostatic shock at the heavy ion front. The author's previous studies have emphasized the idea of using target materials with considerably reduced proton density in order to put the spectral peak at a higher energy, although the energy of the spectral peak will probably not be able to exceed the maximum proton energy reached by a high proton density target [11]. This approach shall henceforth be referred to as the 'proton density reduction' (PDR) scheme. Although the energy of the spectral peak increases with decreasing proton density, it is also clear that the total number of protons available for acceleration decreases as the proton density is decreased. Therefore there must be a proton density at which one produces a spectral peak which contains just as many protons in the same energy range as the broad spectrum produced by a normal target. Beyond this point the PDR scheme provides no further benefit as the number of protons in the spectral peak will always be smaller than the number accelerated by a conventional target. This density shall be referred to as the 'gain limit' (GL). On this basis, one very important question must be: 'What is the GL and how does it scale across a broad range of laser parameters?'. The PDR scheme has not yet been studied across a wide enough range of laser and target parameters to provide a definitive answer to this question.

In this paper we present the results of a scaling study which significantly improves our understanding of how the PDR scheme scales with both laser parameters and target composition. Three different intensity regimes are considered: 10^{19} , 10^{20} and 10^{21} W cm⁻². The targets are considered to have fixed heavy ion density and the proton density is varied between $80n_{\text{crit}}$ and $0.1n_{\text{crit}}$. Note that throughout we generally assume an irradiating wavelength of $1\ \mu\text{m}$, and the critical density (n_{crit} or n_c) is the critical density at this wavelength. It will be shown that the GL seems to lie in the range of proton concentrations of $1n_c < n_p < 5n_c$. Close to the GL, peaks in the energy spectrum are produced which are at 70% of the cut-off energy. This shows that the PDR approach can lead to significant improvements in the energy of the spectral peak over current experiments where the peak energy often lies at less than half of the cut-off energy [2].

The paper is organized as follows: in section 2, some of the basic elements of plasma expansion theory for both one and two ion species which are particularly pertinent to this paper are described. In section 3 both the numerical code and the simulation results for the 1D simulation study are described, and it is shown what region of parameter space needs to be investigated in detail in 2D. In section 4 2D PIC simulations are presented, and in section 5 3D PEPC simulations are presented, both of which show that the validity of the conclusions of section 3 are not drastically changed by multi-dimensional effects.

2. Theory

The mechanism that is thought to be responsible for the acceleration of proton to MeV energies in most current laser–solid experiments is the target normal sheath acceleration (TNSA) mechanism [16]. In qualitative terms, TNSA is the acceleration of ions by strong, quasi-static electric fields that are generated by the charge separation created by highly energetic electrons as they attempt to escape into the vacuum. The simplest analytical model that has been used to

describe TNSA is a 1D self-similar model by Gurevich *et al.* A model by Mora [17] modifies this to include an accurate description of the high energy cut-off in the isothermal case. This model has been further developed, and other analytical models exist [18–22], but it will suffice to describe a fairly simple model.

Consider a 1D scenario consisting of a semi-infinite plasma ($x < 0$) and a semi-infinite vacuum ($x \geq 0$). The plasma is assumed to be collisionless and to consist of a single ion species. It is assumed that the electron population is Maxwellian and is isothermal at temperature, T_e . It is also assumed that quasi-neutrality is maintained throughout. The ion dynamics are described by fluid equations:

$$\frac{\partial n_i}{\partial t} + \frac{\partial n_i u_i}{\partial x} = 0, \quad (1)$$

$$\frac{\partial u_i}{\partial t} + u_i \frac{\partial u_i}{\partial x} = -\frac{Ze}{m_i} \frac{\partial \phi}{\partial x}. \quad (2)$$

Solutions to this set of equations can be sought in terms of a ‘self-similar’ variable $z = x/t$. A boundary condition must be applied, and that is that plasma beyond $x = -c_s t$ (where $c_s = \sqrt{Zk_B T_e/m_i}$) must be undisturbed. The solutions that are then found (for $x > -c_s t$) are

$$u_i = c_s + \frac{x}{t}, \quad (3)$$

$$n_i = n_{i,0} \exp\left(-\frac{x}{c_s t} - 1\right). \quad (4)$$

These solutions naturally imply a broad energy spectrum, and a uniform electric field with a $1/t$ temporal dependence. The assumption of quasi-neutrality needs to be addressed as this may appear to be a dubious assumption, and because these solutions cannot hold at very early times when the plasma density is still close to its initial step-like profile. Numerical simulations have shown that at very early times quasi-neutrality does not hold and the dynamics are dominated by the formation of a strong sheath field. This is only a transient stage, however, as the space charge of the accelerated protons quickly modifies the electric field. A large number of numerical simulations show that at late times these solutions describe the important features of the accelerated protons very well: a linear profile in $p_x - x$ space, an exponential density profile, and a ‘plateau’ in the electric field. A sheath field still exists around the proton–vacuum interface however—the quasi-neutral theory does not describe this.

This basic theory needs to be modified for three important cases: (i) two temperature electron distribution, (ii) at least two ion species and (iii) finite total fast electron energy. The case of a two temperature electron distribution, particularly in the case that is very relevant to current laser–plasma experiments where $T_{\text{cold}} \ll T_{\text{hot}}$, it can be shown that an electrostatic shock must form which effectively separates the hot and cold electrons. A good description of this is given in [12]. In the case of two ion species the termination of the heavy ion density at the heavy ion front causes an abrupt change in the total ion charge density over a very small scale-length—much less than the Debye length. Since quasi-neutrality cannot be maintained at this point, a sheath field forms. This has an effect on the lighter ion species—this causes an accumulation in phase space that produces a peak in the energy spectrum. A more thorough description of this can be found in the literature [11, 12, 14, 15]. If the proton density is comparable to heavy ion density then this process is a fairly small modification to the plasma expansion—a high energy tail is still formed in the energy spectrum. However, if the proton density is very low compared with the heavy ion density then the situation is quite different. The protons will behave in a test-particle-like fashion. This leads to a strong peak in the energy spectrum, and there is little development of a high energy tail. One would expect that the ‘GL’

Table 1. Parameters employed in runs A–L. Note that $n_{C^{4+}} = 40n_c$.

Run	I (W cm ⁻²)	n_p (m ⁻³)	n_p/n_c	Run	I (W cm ⁻²)	n_p (m ⁻³)	n_p/n_c
A	10^{19}	8×10^{28}	80	G	10^{20}	8×10^{28}	80
B	10^{19}	4×10^{28}	40	H	10^{20}	4×10^{28}	40
C	10^{19}	2×10^{28}	20	I	10^{20}	2×10^{28}	20
D	10^{19}	1×10^{28}	10	J	10^{20}	1×10^{28}	10
E	10^{19}	1×10^{27}	1	K	10^{20}	1×10^{27}	1
F	10^{19}	1×10^{26}	0.1	L	10^{20}	1×10^{26}	0.1

that this paper is concerned with would occur close to the onset of this regime. The fact that the total fast electron energy is always finite ultimately limits the ion energies that can be achieved experimentally. A number of studies have looked beyond the isothermal approximation to examine to what extent this limits the maximum ion energy [18, 23]

3. 1D simulation study

3.1. Numerical code

The numerical code employed in the 1D simulation study is a 1D3P electromagnetic particle-in-cell (PIC) code that was previously used in the study reported in [24]. This code uses standard explicit PIC methods [25]. Linear interpolation is used for particle and grid weighting, and the electric field obeys Gauss' Law. In the simulations a grid of 100 000 spatial points was used with a cell size of 2×10^{-9} m. A foil target with a thickness of $1 \mu\text{m}$ was placed at $x = 100 \mu\text{m}$. The electron temperature was set to 20 keV. The heavy ion species used was either C^{4+} or D^+ at a density of $4 \times 10^{28} \text{ m}^{-3}$ ($40n_{\text{crit}}$) throughout the target. The proton density was also uniform throughout the target, the densities used in each run are given in table 1. This ensured a minimum electron density of either $1.6 \times 10^{29} \text{ m}^{-3}$ ($160n_{\text{crit}}$) or $4 \times 10^{28} \text{ m}^{-3}$. C^{4+} was chosen as it is usually the highest charge state of carbon observed in many experiments [26].

In all runs the temporal profile of the 'laser' pulse was defined by a \sin^2 envelope function, with a total length of $2ct_{\text{pulse}}$. The pulse duration was set to $t_{\text{pulse}} = 80$ fs, and a wavelength of $1 \mu\text{m}$. 2×10^6 quasi-particles were used for each species, ensuring that the initial number of particles per cell was 4000. The simulations were run up to 400 fs.

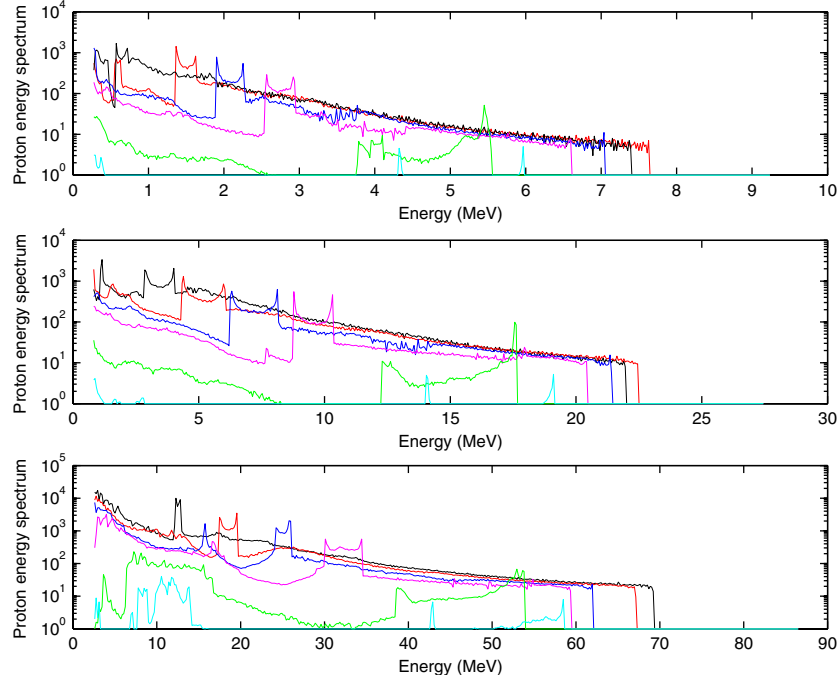
3.2. Results

Initially three sets of six runs were carried out, using the set-up described in section 3.1, labelled A–R. Runs A–F used a laser pulse with a full width at half maximum (FWHM) intensity of $1 \times 10^{19} \text{ W cm}^{-2}$ and proton densities of 8×10^{28} , 4×10^{28} , 2×10^{28} , 1×10^{28} , 1×10^{27} and $1 \times 10^{26} \text{ m}^{-3}$, respectively. Runs G–L used a laser pulse with a FWHM intensity of $1 \times 10^{20} \text{ W cm}^{-2}$ and runs M–R used a laser pulse with a FWHM intensity of $1 \times 10^{21} \text{ W cm}^{-2}$ both with the same set of proton densities as A–F. The simulation parameters are tabulated in tables 1 and 2, including the percentage of protons by number density in table 2. For runs A–R the heavy ions species used was C^{4+} . The target therefore represents a polymer target.

The spectra at 300 fs for runs A–R have been compiled in three plots in figure 1. Figure 1 shows that the same variation with proton density is observed in all three intensity regimes. The peak in the proton spectrum is seen to increase as the proton density decreases, and the

Table 2. Parameters employed in runs M–R. Note that $n_{C^{4+}} = 40n_c$.

Run	I (W cm^{-2})	n_p (m^{-3})	n_p/n_c	% protons
M	10^{21}	8×10^{28}	80	67
N	10^{21}	4×10^{28}	40	50
O	10^{21}	2×10^{28}	20	33
P	10^{21}	1×10^{28}	10	20
Q	10^{21}	1×10^{27}	1	2.4
R	10^{21}	1×10^{26}	0.1	0.25


Figure 1. Proton energy spectra as a function of intensity and initial proton density. Top plot is for $I = 10^{19} \text{ W cm}^{-2}$, Middle is for $I = 10^{20} \text{ W cm}^{-2}$ and Bottom is for $I = 10^{21} \text{ W cm}^{-2}$. Colour coding: $n_p = 80n_{\text{crit}}$ black; $n_p = 40n_{\text{crit}}$ red; $n_p = 20n_{\text{crit}}$ blue; $n_p = 10n_{\text{crit}}$ magenta; $n_p = 1n_{\text{crit}}$ green; $n_p = 0.1n_{\text{crit}}$ cyan.

maximum proton energy decreases as the proton density decreases. This is in good agreement with what has been observed in previous work [11, 10].

What is interesting is that at all three intensities one finds that the GL appears to be a proton density slightly less than $n_p = n_c = 1 \times 10^{27} \text{ m}^{-3}$ (relative fraction of 2.4%). This allows for very substantial gains in peak energy over a baseline of a 1 : 1 composition—4 MeV in the $10^{19} \text{ W cm}^{-2}$ case, 10 MeV in the $10^{20} \text{ W cm}^{-2}$ case and 33 MeV at $10^{21} \text{ W cm}^{-2}$. Expressed as fractions of the maximum proton energy (i.e. the energy of the sharp cut-off at $n_p = 8 \times 10^{28} \text{ m}^{-3}$) we find that $\epsilon_{\text{pk}}/\epsilon_{\text{max}}$ goes from 0.2 to 0.25 at the 1 : 1 baseline up to 0.7–0.75 at the GL.

The result of the simulations can also be seen in the form of a peak energy scaling with intensity, which is plotted for three compositions ($n_p = 1, 10$ and $40n_{\text{crit}}$) in figure 2. It was found that at all compositions the scaling with intensity is well fitted by an expression of

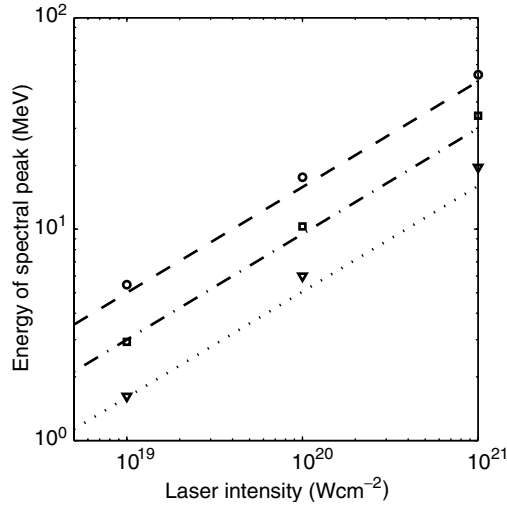


Figure 2. Scaling of the energy of the spectral peak with laser intensity for $n_p = n_{\text{crit}}$ (circles), $n_p = 10n_{\text{crit}}$ (squares), $n_p = 40n_{\text{crit}}$ (triangles). Lines are approximate scaling expressions: $\epsilon_{\text{pk,MeV}} = 5I_{19}^{1/2}$ (dashed), $\epsilon_{\text{pk,MeV}} = 3I_{19}^{1/2}$ (dash-dot) and $\epsilon_{\text{pk,MeV}} = 1.6I_{19}^{1/2}$ (dotted).

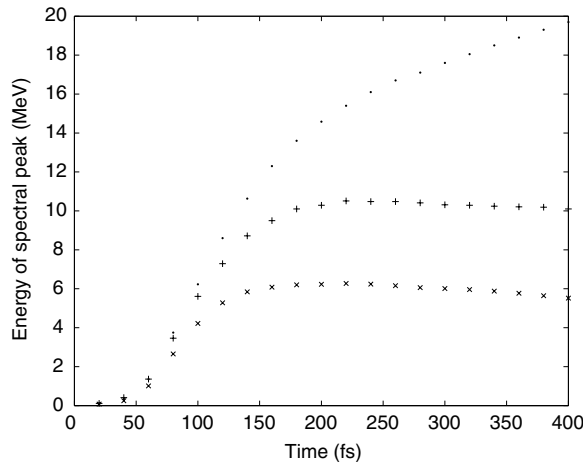


Figure 3. Energy of the spectral peak as a function of time in runs H (crosses), J (plus signs) and K (dots).

the form $E_{\text{pk,MeV}} \propto I_{19}^{1/2}$, where I_{19} is the laser intensity in units of $10^{19} \text{ W cm}^{-2}$. In a 1D calculation this is reasonable finding. The velocity of the heavy ion front is proportional to the ion acoustic velocity ($v_i \propto c_s$) and since the proton bunch that produce the peak are travelling close to this velocity the energy of the spectral peak is expected to scale as $E_{\text{pk}} \propto T_{\text{fast}}$. The fast electron temperature is expected to scale as $T_{\text{fast}} \propto I^{1/2}$.

The reader may well be interested to know to what extent these spectra represent the asymptotic state of the plasma expansion. To show this we have plotted the energy of the spectral peak as a function of time in runs H, J and K in figure 3. Since the spectral peaks take the form of a ‘tower’ we measure the peak energy from the upper edge of the ‘tower’. Figure 3

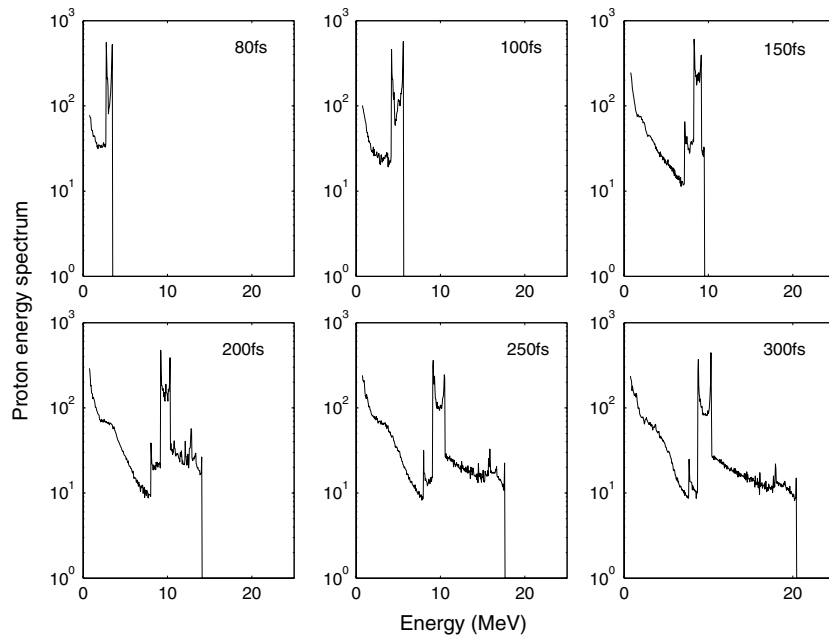


Figure 4. Proton energy spectrum of run J at 80, 100, 150, 200, 250 and 300 fs.

is representative of the behaviour at the other two intensities. At high proton concentration the energy of the spectral peak reaches a maximum close to 200 fs and the peak energy then declines slightly at later times. At very low proton concentrations the peak energy is still increasing at 400 fs. In figure 4 the proton energy spectrum of run J is plotted at six different times to illustrate the evolution of the energy spectrum during the simulation.

Figure 4 shows that the spectral peak is formed early and accelerates up to 10 MeV by 200 fs, after this time the peak energy decreases slightly, but the maximum proton energy continues to increase as a high energy, exponential tail is formed in the spectrum. The crucial event in the formation of the spectral peak is the point at which the energy at which the peak sits stops increasing at the exponential tail forms. At high proton concentrations (e.g. run A) this occurs very quickly and the peak is not strong. However, for low concentrations the tail formation occurs later, and the peak is much stronger. The exponential tail is due to expansion of protons beyond the C^{4+} front in a fast rarefaction wave (i.e. self-similar expansion). This is representative of the general, qualitative temporal evolution of the energy spectrum throughout runs A–R.

It is worthwhile to use the simulation results to describe the physical mechanism that is forming the spectral peak. The ion densities, charge density and electric field output from run J are used to show this in figure 5. What this shows is that the electric field consists of a uniform region and two sheath fields which, by comparison with the density plots, one can see are associated with the heavy ion front and the proton front. Although the electric field and ion densities evolve throughout the simulation this snapshot illustrates the general features.

To complement this the evolution of the $p_x - x$ proton phase space in run J from 50 to 300 fs is shown in figure 6. This shows that the quasi-monoenergetic bunch sits around $105 \mu\text{m}$ at 200 fs, which means that it lies in a region of low field between the ion fronts (according to figure 5(a)). The mechanism of peak formation can now be understood as follows: the

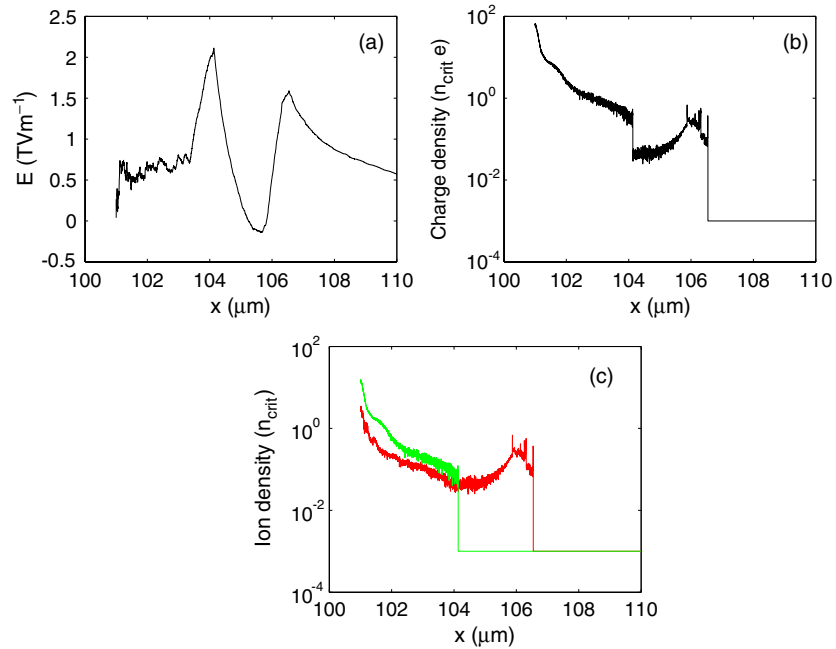


Figure 5. (a) Electric field behind the target in run J at 200 fs in TV m^{-1} . (b) Charge density behind the target in run J at 200 fs in $n_{\text{crit}}e$. (c) Proton density (red) and heavy ion density (green) in run J at 200 fs in $n_{\text{crit}s}$.

termination of the heavy ion density (figure 5(c)) implies a very sharp change in the charge density (figure 5(b)). Quasi-neutrality cannot be maintained here so the charge separation results in the sheath field (as it does at the proton front). Protons which are accelerated by the sheath field then enter a region of low electric field immediately beyond, and the acceleration is considerably reduced. The effect of this is to create a region of quasi-ballistic flow. On integrating to find the energy spectrum, one then realises that this quasi-ballistic flow is the quasi-monoenergetic bunch that one has been seeking. Note that by the time the peak reaches its maximum energy the heavy ion front will have moved a significant distance from the initial position of the rear surface and that the electron population consists only of fast electrons by this point. The spectral peak formation is not strongly affected by reducing the initial cold electron temperature.

It was previously noted that the spectral peak actually takes the form of a ‘tower’ structure with two very sharp peaks at the high and low energy ends of the structure. Although the peaks are very sharp the actual width (energy difference between the two peaks) of the tower is substantial. In run D it is 0.4 MeV, in run J it is 1.7 MeV and in run P it is 4.5 MeV (all at 300 fs). The cause of this can be seen by examining the proton phase space. Once again, run J is used as an example, and the reader is referred to figure 6. The spectral peak is due to the ‘sine-wave’ like structure in phase space. The sharp peaks are due to the turning points of this structure. The phase space evolution also shows that this is a dynamic entity—protons are accelerated into and out of this structure throughout the simulation. So when it is observed that the peak energy decreases slightly at late times in the simulation, this is not because there is any deceleration as such. This is caused by a reduction in the sudden boost that ‘new’ protons crossing the heavy ion front receive.

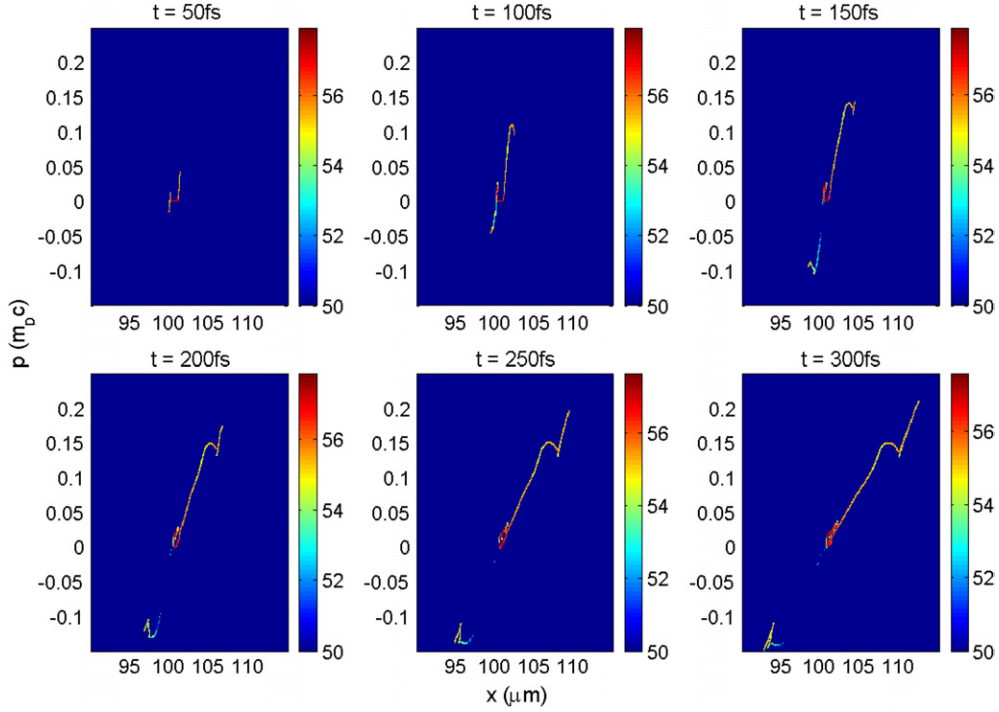


Figure 6. Proton phase space ($x - p_x$) of run J at 50, 100, 150, 200, 250 and 300 fs.

One-dimensional simulations were also used to study the effect of the choice of heavy ion species on the spectral peak. There is a considerable difference between C^{4+} and C^{6+} , and this was found by repeating runs D, J and P ($n_p = 10n_{crit}$) with C^{6+} as the heavy ion species (the new runs are labelled S, T and U, respectively). The proton energy spectra at 300 fs are shown in figure 7 alongside the proton energy spectra of runs D, J and P.

It is clear from runs S–U that the spectral peak is much narrower and is located at a higher energy. The FWHM width of the peak at 300 fs in run S is 0.1 MeV and in runs T and U it is 0.5 MeV and 1 MeV, respectively. This is an improvement of a factor of 4. The higher energy is certainly expected since increasing the charge-to-mass ratio of the heavy ions must increase the velocity of the heavy ion front, since $v_i \propto c_{s,i}$. These runs suggest that using deuterium as a secondary ion species (i.e. in a CD–CH target) may be better for producing narrow spectral peaks.

From these 1D studies it was found that all three intensity regimes exhibited similar behaviour. Importantly, the GL appears to lie in the range $n_p \approx 0.1 - 1n_c$ in all three intensity regimes. This implies that it is only really necessary to determine the GL for one intensity. Therefore it is the lowest proton concentrations that need to be studied in 2D and 3D simulations at a single intensity to improve our determination of the GL.

In this study we have not considered the thickness of the source region in any detail. In the 1D runs the target composition was uniform throughout the foil. From a few 1D and 2D runs it was found that for most target compositions, setting the source layer thickness $> 0.1 \mu m$ does not significantly alter the formation of the spectral peak (either width or energy of the peak). In [11] it was found that reducing the source layer to 10 nm improved the spectrum produced at low proton concentrations by eliminating low energy protons (not ones in the spectral peak).

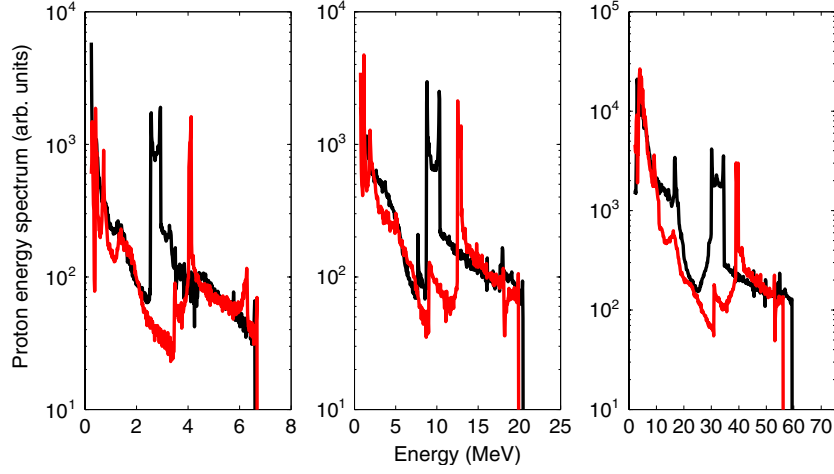


Figure 7. Proton energy spectra at 300 fs of runs repeated with C^{6+} as the heavy ion species (red) compared with the proton energy spectrum of the original run: run S (cf D), run T (cf J), run U (cf P).

Table 3. Parameters employed in 2D simulations.

Run	I ($W\text{ cm}^{-2}$)	n_p/n_c	n_i/n_c	% protons
1	10^{21}	1	79	1.25
2	10^{21}	5	75	6.25
3	10^{21}	10	70	12.5
4	10^{21}	60	20	75

However, even at 10 nm thickness, at high proton concentration a broad, exponential spectrum was still produced.

4. 2D simulation study

4.1. Numerical code

The numerical code used to perform 2D simulations is the 2D3POSIRIS code [27]. Simulations were performed on a spatial grid of 8000×8000 cells with each cell being $0.16c\omega_1^{-1}$ (25 nm) square. The target consisted of a slab of proton-free substrate material with a proton-bearing microdot on the rear surface. The slab of substrate material was $10\ \mu\text{m}$ wide and $1\ \mu\text{m}$ thick, and it consisted of ions with a charge-to-mass ratio of 3660 at a density of $80n_{\text{crit}}$, with an equal electron density to give initial charge neutrality. The microdot was centred in y and was $4.8\ \mu\text{m}$ wide and was $0.32\ \mu\text{m}$ thick, and it consisted of a mixture of protons and ions with a charge-to-mass ratio of 3660. The exact composition in the various runs is given in table 3. In each cell there were 64 quasi-particles representing the electrons, 64 representing protons and 32 representing heavy ions.

The laser pulse enters from the left-hand side of the grid and is normally incident on the centre of the front side of the substrate foil. The pulse has a triangular temporal profile with a total pulse duration of 80 fs. The FWHM intensities in each run are given in table 3. The transverse spatial profile of the pulse is Gaussian, with a $1/e$ width of $40c\omega_p^{-1}$ ($6.4\ \mu\text{m}$).

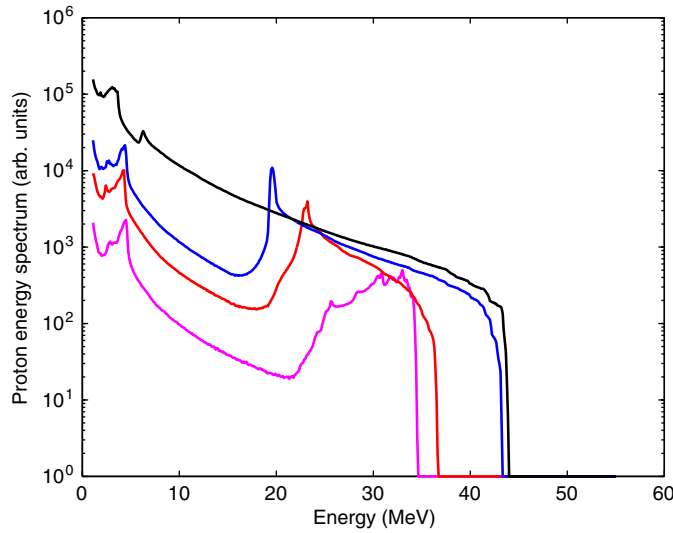


Figure 8. Proton energy spectra of 2D runs (1–3) at 250 fs: run 1 = magenta line ($n_p = 1n_c$), run 2 = red line ($n_p = 5n_c$), run 3 = blue line ($n_p = 10n_c$), run 4 = black line ($n_p = 60n_c$).

Simulations were run up to 250 fs. Beyond this time the highest energy protons start colliding with the far boundary of the simulation box.

4.2. Results

Four simulations were carried out for a FWHM intensity of $10^{21} \text{ W cm}^{-2}$, the runs being labelled 1–4. The microdot compositions are given in table 3. The proton energy spectra for the three runs are plotted in figure 8. The FWHM of the spectral peak in run 3 is 0.55 MeV.

Figure 8 shows that the main conclusion drawn regarding the GL from the 1D simulations, also holds in 2D calculations. The GL appears to lie in the range $1 < n_{p, \text{GL}}/n_{\text{crit}} < 5$, which agrees well with what is seen in 1D (see section 3).

It is interesting to examine the physical behaviour of the different microdots in the 2D simulations which underpins the differences in the energy spectra. Figure 9 shows the proton density, heavy ion density and E_x component of the electric field of runs 2–4 at 150 fs. This shows that, in the case of runs with initially low proton concentrations, the proton density dips and then rises beyond the heavy ion front. In the longitudinal (E_x) component of the electric field, there is a peak in the electric field associated with the heavy ion front and the proton front. This is very similar to what is found in 1D simulations (see figure 5). In the run with initially high proton concentration (run 4), the heavy ions are not significant and no spectral peak is generated. In this case the proton density profile is an exponential decay up to a sharp cut-off, and the electric field is uniform in the slope, with a sheath field at the proton front. This is the mode of proton acceleration via plasma expansion that is thoroughly reported in the literature. It can therefore be said that not only do our conclusions concerning the GL apply in 2D as well as 1D, but our conclusions about the physical mechanism do as well.

Two-dimensional simulations also provide information about the angular beam properties of the accelerated protons. This is done by recalculating the spectrum and accepting only those protons which are travelling within an angle to the laser axis of ϕ_{obs} of less, i.e. one imagines that this is the acceptance angle of a distant collimator hole. This was done for runs 3 and 4, for the case of $\phi_{\text{obs}} = 2^\circ$, and the results are shown in figure 10.

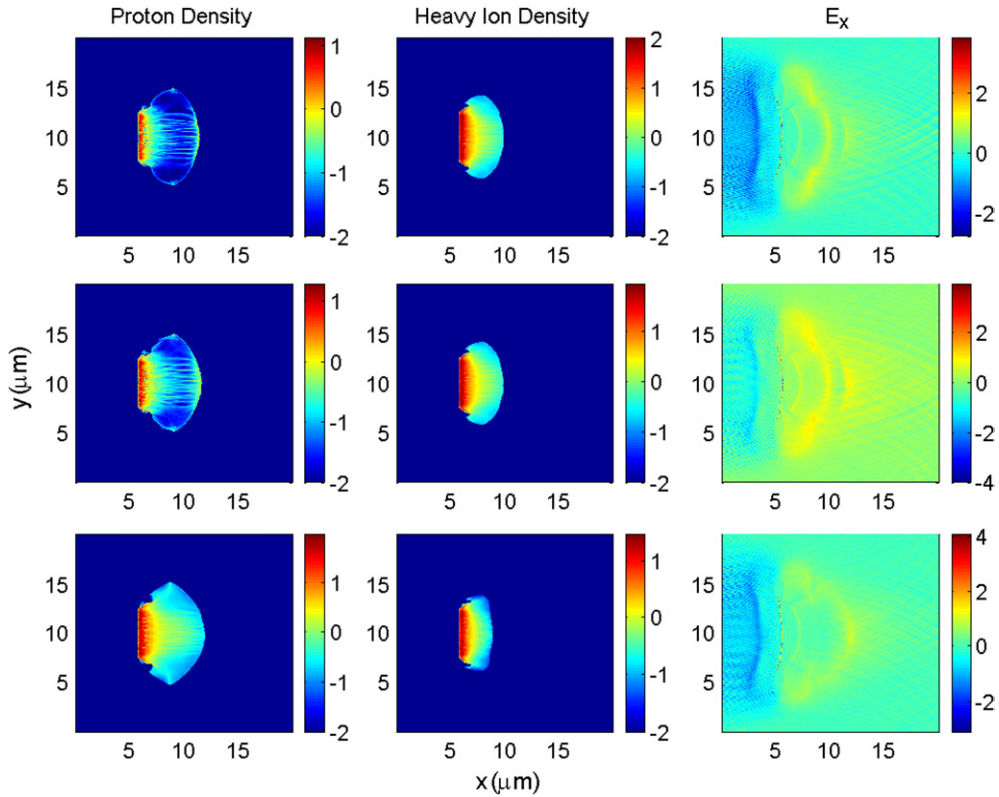


Figure 9. Proton density ($\log_{10}(n_p/n_c)$) (left column), heavy Ion density ($\log_{10}(n_i/n_c)$), and E_x component of electric field of runs 2 (top row), 3 (middle row) and 4 (bottom row) at 150 fs. Note changes in colour scale.

What figure 10 shows is that at high proton concentration, the spectrum of all the protons and those at very low divergence is only really different by a factor which is the same for most energies. At low proton concentration the same applies for most energies. However, the spectral peak of the very low divergence protons has a slightly narrower energy spread and is better defined in the sense that the difference between the maximum signal and the signal at which the spectrum becomes quasi-Maxwellian again is larger. The ratio between the maximum signal of the spectral peak at the signal at the same energy of run 4 also increases when one selects the low divergence protons—from 3.7 to 5.6.

5. 3D simulation study

5.1. Numerical code

The numerical code used here is the pretty efficient parallel Coulomb solver (PEPC) [28, 29]. PEPC is a gridless particle code that directly solves for the Coulomb force between quasi-particles using multipole expansions to reduce the number of operations in the force summation to $O(N \log N)$. Wave propagation is neglected and the code is purely electrostatic. Laser absorption is included by means of a ponderomotive model, which includes both $v \times B$ heating and profile steepening at the critical surface. Comparisons with 2D electromagnetic

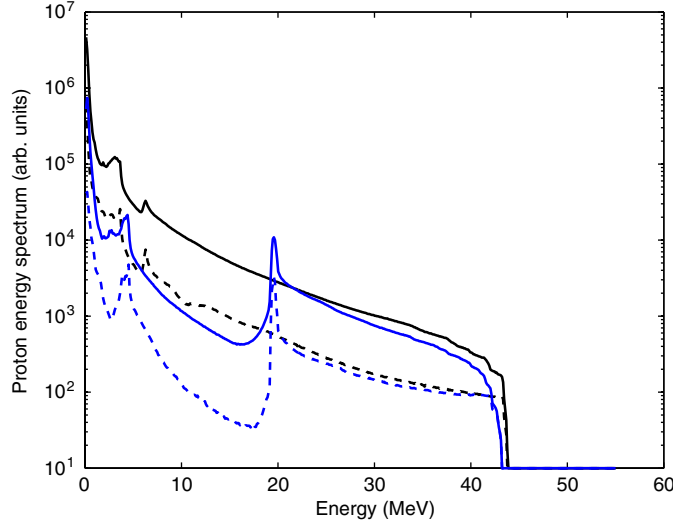


Figure 10. Proton energy spectra of runs 3 and 4 at 250 fs showing spectra of all protons and protons travelling at $\theta < 2^\circ$: blue dashed = run 3 ($\theta < 2^\circ$), blue solid = run 3 (all), black dashed = run 4 ($\theta < 2^\circ$), black solid = run 4 (all).

PIC simulations show that the interaction physics is accurately described for ‘rigid’, overdense targets such as those considered here [29]. Moreover, the gridless paradigm permits true free-space boundary conditions, avoiding artificial confinement of the hot electron cloud to a finite simulation box and possible unphysical distortion of the accelerating field seen by the ions. The configuration that was employed in this study is very similar to that used in [10], and we extended that study to examine the low proton concentration limit at three different intensities (these runs being labelled I–III).

The initial configuration consists of a foil target of size $3.14 \times 1000 \times 1000 c^3 \omega_p^{-3}$ ($\approx 0.1 \times 30 \times 30 \mu\text{m}^3$), with an electron density of $16 n_{\text{crit}}$. The plasma ions are He^+ ions ($Z = 1$, $A = 4$), the electron temperature is initially 300 eV and the ions are initially cold. The protons are present as a microdot of transverse dimensions $200 \times 200 c^2 \omega_p^{-2}$ which is centred and which extends $1 c \omega_p^{-1}$ from the rear surface ($\approx 30 \text{ nm}$). The microdot consists purely of protons at a density of $0.8 n_{\text{crit}}$. An equal density of electrons is also added so that the target is initially charge neutral. The spatial extent of the quasi-particles, ϵ , is set to $3 c \omega_p^{-1}$. This means that the plasma is effectively collisionless, which simplifies the initialization of the simulation. The simulations were run up to $3000 \omega_p^{-1}$ ($\approx 300 \text{ fs}$).

In all runs a laser pulse with a wavelength of 800 nm, a pulse duration of 35 fs (FWHM) and a focal spot radius of $150 c \omega_p^{-1}$ ($\approx 4.8 \mu\text{m}$) was modelled. In run I the amplitude of the normalized vector potential was set to $a_0 = 2.7$, in run II it was set to $a_0 = 8.5$ and in run III it was set to $a_0 = 19$.

5.2. Results

The proton energy spectra of the runs at $1000 \omega_p^{-1}$ (106 fs) are plotted in figure 11. This demonstrates that essentially the same results are found in 3D calculations as they are in the 1D and 2D calculations in terms of producing quasi-monoenergetic bunches at very low proton densities across a wide range of intensities. The energies of the spectral peaks are plotted against the laser intensity in figure 12, also plotted is the expression $\epsilon_{\text{pk,MeV}} = 5 I_{19}^{1/2}$.

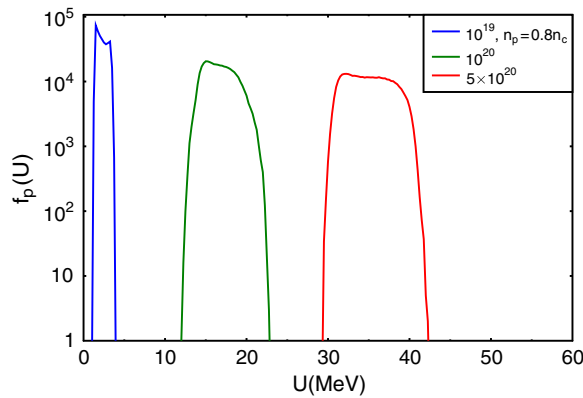


Figure 11. Proton energy spectra from 3D PEPC simulations.

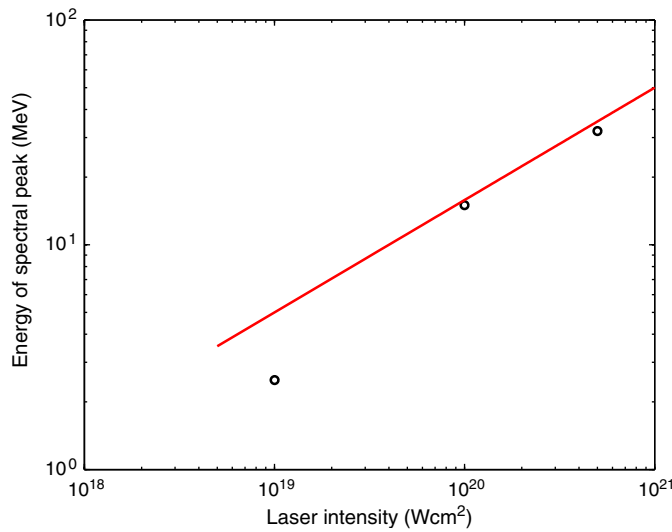


Figure 12. Energy of spectral peak in 3D PEPC simulations versus laser intensity (black circles). The red line is a plot of $\epsilon_{pk,MeV} = 5I_{19}^{1/2}$.

Although the proton spectra shown in figure 11 have a relatively low energy spread compared with proton spectra from targets with a very high proton concentration (cf figure 1), they do not exhibit the strong and narrow peak formation observed in the other runs presented in this paper. This can be attributed to the fact that, in these simulations, the microdot is extremely thin (30 nm). Under these conditions the protons very quickly completely separate from the ions. Once the protons have completely separated from the ions the heavy ion front cannot act to dynamically maintain the bunched population of ions. Without this the energy spread of the proton bunch increases due to temporal and spatial variation in the fast electron sheath and because of the space charge of the proton bunch itself. Since the microdots are very thin, almost all of the protons are accelerated, thus leaving no low energy protons in marked contrast to the other spectra presented in this paper. This effect was also observed in previous work [11].

Therefore very thin microdots ($\approx 10\text{--}50$ nm) may be a less optimal choice than current microdots (> 100 nm). This set of runs therefore supports the same observation made in earlier work [10].

6. Summary and conclusions

An extensive set of numerical simulations using 1D and 2D PIC codes and a 3D tree code have been carried out to study the generation of quasi-monoenergetic proton bunches from microdot targets with a low proton concentration. In contrast to other work, this study has aimed to look at a broad range of intensities and target compositions, with particular emphasis on determining the concentration below which the PDR approach is no longer beneficial (i.e. the ‘GL’). The specific conclusions of this study can be summarized as follows.

- (i) The changes in the energy spectrum and the increase in the spectral peak’s energy as the proton concentration in the target/microdot is decreased followed the same general pattern in all three intensity regimes and in all three of the simulation tools used.
- (ii) The ‘GL’ was found to lie within the region of $1\text{--}5n_{\text{crit}}$ in the 10^{21} W cm $^{-2}$ regime, and in the region of $0.1\text{--}1n_{\text{crit}}$ in the $10^{19}\text{--}10^{20}$ W cm $^{-2}$ regime. This means that by using the PDR approach, spectral peaks with energies up to 50% and 75%, respectively, of the maximum proton energy accessible by TNSA can be produced in a more efficient manner than by using standard TNSA and employing a post-acceleration energy selection technique.
- (iii) In both the 1D and 3D simulations the scaling of the energy of the spectral peak with laser intensity was well described by an expression of the form $\epsilon_{\text{pk,MeV}} = CI_{19}^{1/2}$ for all target compositions (C is a constant determined by the composition).
- (iv) In the 1D simulations it was found that a target composed of a hydrogen–deuterium mix produced spectral peaks with a much lower energy spread than targets composed of mixture of hydrogen and lower charge-to-mass ratio species.

This therefore leads one to two general conclusions. Firstly that microdot targets with a low (order $1n_{\text{crit}}$) proton density are a promising route to generating quasi-monoenergetic proton beams which can reach a large (> 0.7) fraction of the maximum energy that TNSA can achieve for a given laser–target configuration and contain more protons than could be obtained by post-selection from a conventional TNSA spectrum. This may lead to immediate improvements over current experimental results such as those reported in [2]. Secondly the fact that the general dependence on the proton concentration is similar in all three intensity regime implies that experimental work results obtained on multi-TW ‘table-top’ systems should readily scale to much higher energy laser systems (e.g. POLARIS at IOQ Jena or ASTRA-GEMINI at RAL). However, it should be noted that a full experimental investigation of the PDR scheme will require the development of methods for manufacturing microdots with low proton concentrations (ranging from the development of special organic polymers to ion implantation techniques). Future theoretical work will have to address the issue of the width of the spectral peak and to study the expansion over a longer duration.

Acknowledgments

We are grateful for the use of computing resources provided by Science and Technology Facilities Council’s e-Science facility, and the Juelich Supercomputing Centre under VSR Project JZAM04. SMP and OJ are funded by the Deutsche Forschungsgemeinschaft (DFG) within the transregional Collaborative Research Center ‘Relativistic Laser Plasma Dynamics’

under contract TR18. JP is funded by the Bundesministerium für Bildung und Forschung (BMBF) within the Center for Innovation Competence ‘Ultra Optics’. The authors gratefully acknowledge fruitful discussions concerning the experimental issues with H Schwoerer, R Sauerbrey, K Ledingham, W Galster, M Kaluza and D Neely.

References

- [1] Schwoerer H *et al* 2006 *Nature* **439** 445
- [2] Pfoth S M *et al* 2008 *New J. Phys.* **10** 033034
- [3] Hegelich M *et al* 2006 *Nature* **439** 441
- [4] Ter-Avetisyan S *et al* 2006 *Phys. Rev. Lett.* **96** 145006
- [5] Toncian T *et al* 2006 *Science* **312** 410
- [6] Linz U and Alonso J 2007 *Phys. Rev. ST-AB* **10** 094801
- [7] Esirkepov T *et al* 2004 *Phys. Rev. Lett.* **92** 175003
- [8] Zhang X *et al* 2007 *Phys. Plasmas* **14** 073101
- [9] Robinson A P L *et al* 2008 *New J. Phys.* **10** 013021
- [10] Robinson A P L and Gibbon P 2007 *Phys. Rev. E* **75** 015401
- [11] Robinson A, Bell A and Kingham R 2006 *Phys. Rev. Lett.* **96** 035005
- [12] Tikhonchuk V T *et al* 2005 *Plasma Phys. Control. Fusion* **47** B869
- [13] Wickens L and Allen J E 1978 *Phys. Rev. Lett.* **41** 243
- [14] Bychenkov V Y *et al* 2004 *Phys. Plasmas* **11** 3242
- [15] Brantov A V *et al* 2007 *Phys. Plasmas* **13** 122705
- [16] Wilks S C *et al* 2001 *Phys. Plasmas* **8** 542
- [17] Mora P 2003 *Phys. Rev. Lett.* **90** 185002-1–185002-4
- [18] Mora P 2005 *Phys. Rev. E* **72** 056401
- [19] Dorozhkina D and Semenov V 1998 *Phys. Rev. Lett.* **81** 2691
- [20] Murakami M and Basko M 2006 *Phys. Plasmas* **13** 012105
- [21] Fuchs J *et al* 2006 *Nature Phys.* **2** 48
- [22] Schreiber J *et al* 2006 *Phys. Rev. Lett.* **97** 045005
- [23] Betti S *et al* 2005 *Plasma Phys. Control. Fusion* **47** 521
- [24] Robinson A P L, Neely D, McKenna P and Evans R G 2007 *Plasma Phys. Control. Fusion* **49** 373–84
- [25] Birdsall C K and Langdon A B 1991 *Plasma Physics via Computer Simulation* (Hilger: New York)
- [26] Hegelich M *et al* 2005 *Phys. Plasmas* **12** 056314
- [27] Lee S 1988 *Phys. Rev. E* **61** 1074
- [28] Gibbon P 2005 *Phys. Rev. E* **72** 026411
- [29] Gibbon P, Beg F, Evans R, Clark E and Zepf M 2004 *Phys. Plasmas* **11** 4032